Hindawi Publishing Corporation
Smart Materials Research
Volume 2012, Article ID 530217, 9 pages
doi:10.1155/2012/530217

Research Article

Thermaly Active Structures for Shape Morphing Applications

Gildas L'Hostis, Karine Buet-Gautier, and Bernard Durand

Laboratoire de Physique et Mécanique Textiles de Mulhouse, Ecole Nationale Supérieure d'Ingénieur de Sud Alsace, 11 rue Alfred Werner, 68093 Mulhouse, France

Correspondence should be addressed to Gildas L'Hostis, gildas.lhostis@uha.fr

Received 15 January 2012; Accepted 7 March 2012

Academic Editor: Sontipee Aimmanee

For shape morphing application, thermal activation coupling to a bimetallic strip effect can be a substitute for classical actuators, piezoelectrical or shape memory alloys. The controlled behaviour of composite material (CBCM) is a thermaly activated composite material. The thermal activation is made thanks to carbon yarns which are connected to a power supply. If the anisotropy of the structure is well organized, the desired deformation is reached when the temperature within the composite is rising. To obtain a CBCM morphing composite structure, it is necessary to design a specific structure. The aim of this work is to show that it is possible to adapt the CBCM principle in order to transform any kind of classical composite structure to an active structure. The first part of this work consists in presenting the experimental results for two examples of composite beams. The second part is about the active structure FEM modeling and the development of adapted tools for this particular design.

1. Introduction

Because of their capacity of actuation, morphing structures are used to simplify mechanisms by reducing the number of moving parts. Three main actuation technologies are commonly used: piezoelectricity, shape memory alloys, or thermal effect. In the case of a structure with bistable effect, these technologies are used to activate the shape changing by piezoactuation [1–3], SMA actuation [4–6], and thermal actuation [7–9]. The field of applications for bistable structures is limited because they have only two positions of stability witch are not adjustable and link to the structure geometry.

In the case of standard not bistable composite structures, the main problem is the link between the composite and the actuator. Many works can be found with SMA [10, 11] actuators or piezoactuators like macro-fiber composite (MFC) [12, 13], but the interface strength between the actuator and the composite plays a crucial role in the time life of the structure that is a limit especially when the rigidity of the composite structure is high. To overcome problems of bonding between the actuator and the structure, the bimetallic strip effect coupled to an internal thermal actuation can be a solution. Indeed the whole structure can be considered as an actuator, and the problems of interface decohesion are not concentrated at the interface actuator/structure but distributed all along the interfaces of the laminate composite.

Controlled behaviour composite material (CBCM) [14–18] is a thermal actuator developed ten years ago. There are two different ways to use the CBCM (Figure 1): the first one is called "temperature effect" and the second "gradient effect"; the difference between the two effects is the possibility for the composite structure to bend in one or two directions, respectively. The temperature effect is obtained thanks to an asymmetric laminate made of layers with different coefficients of thermal elongation in a given direction. Then, the deformation of the structure is controlled, at the beginning, by a thermal gradient that can appear through the thickness of the composite structure and, finally, by the temperature when the thermal gradient is established. In contrast with that, the gradient effect can be obtained with any composite structure containing an insulating layer, for example, a sandwich structure. If one side of the composite is heated, as the other side is insulated, a temperature gradient appears within the structure. In this case, the bending deformation is linked only to the thermal gradient value through the thickness of the composite. So the

behaviour of the sandwich structure is similar to the one of a shape memory material because it has only two extreme positions, linked to the nature of the core material [ref].

However, a thermal actuation is not unidirectional like a SMA wire actuation, but multidirectional. The thermal activation of a laminate plate induces curves along the two dimensions of the plate. To get a maximal bending in one direction, it is necessary to soften the curve in the other direction, because this curvature induces a geometrical rigidity. Therefore a compromise between the longitudinal and the transversal thermal expansion coefficients of each layer of the laminate must be found.

One solution is to use a quasi-isotropic layer and adapt the transversal property of the other layers. Asanuma et al. [18] used this solution and presents an active composite made of composite/metal layers. To create the thermal field, a CFRP (unidirectional carbon-fiber-reinforced plastic) connected to a current generator was used. The CBCM does not use metallic material (except for the electrical connections), but only classical composite materials: carbon yarns connected to a power supply are used to heat the structure. Two solutions are used to reduce the undesired curves. The first one is to choose optimum reinforcements, in terms of kind, orientation, and placement. For a plate in bending along its longitudinal axis, the addition, at the level of the mean plane, of a unidirectional carbon in the direction of the transverse axis will soften the curve [15]. The second solution is to increase the slenderness of the structure or of the thermal activation area. Compared to a MFC or composite incorporating SMA wires, the manufacturing of a CBCM is very easy and compatible with conventional manufacturing processes of composites. However, the composite structure must be designed especially in terms of shape and constitution. The objective of this work is to show that any nonactive composite structure can be turned into an active one without changing its initial geometry, but only by adding a CBCM patch.

In the first part of this paper, the composite structures, experimental procedure, and method to characterize the mechanical performance are presented. The second part is about the development of a model (Abaqus software) adapted to the computation of this kind of structure.

2. Thermal Local Activation

2.1. Material and Methods. Two composite structures made of two parts are tested. The first part is a beam ($300 \times 50 \times e$ mm^3), and the second part is a patch. In order to study the influence of the beam stiffness, we used two different beams. The first one is made of three plain weave glass fabrics ($2D^G$); the thickness of the fabric is 0.2 mm and the mass per unit area is 200 g/m^2. The second beam is made of two unidirectional fiber glass (UD^G); the thickness is 0.7 mm and the mass per unit area is 650 g/m^2. In this last case, the beams are cut in order to have the UD axis along the transverse axis.

The matrix is an epoxy resin, Epolam 2025 from Axson; the process, particularly the curing cycle, is the one recommended by the manufacturer to obtain a temperature of glass transition of 135°C.

Table 1: Structure properties.

Beam	Mass (g)	Volume 10^{-6} m^3	$K\ 10^{-3}$ (N/m)	R_{AL} (Ω)
CBCM-A	35	11.3	0.56	4.93
CBCM-B	48	23.4	1.11	4.37

A local CBCM effect is produced by adding an active composite patch on the beams (Figure 2). This patch (112 mm × 40 mm) is made of two plain weave aramid fabrics ($2D^A$), the thickness of the fabric is 0.5 mm, and the mass per unit area is 230 g/m^2. The active layer (AL) is made of four parallel carbon yarns along the beam direction and is put between the two aramid layers. The structures (beam with patch) have an asymmetric constitution: $({0_{3x\,2D}}^G \setminus {0_{2D}}^A \setminus 0_{AL} \setminus {0_{2D}}^A)$ for the first beam CBCM-A and $({90_{2x\,UD}}^G \setminus {0_{2D}}^A \setminus 0_{AL} \setminus {0_{2D}}^A)$ for the second beam CBCM-B. To have a plane geometry for the final structures, initial beams and active patches are curing separately. Then the patches are bonded using a methacrylate resin; after this step, no supplementary curing are made.

In order to compare the performances of the active structures, two tests of cantilever bending are carried out [19]. When the active parts are powered, the first test consists in measuring the free displacement d_L using a linear variable differential transformer (LVDT) sensor (accuracy: 1/100 mm), at 130 mm from the clamping. The second test consists in locking the beam at 130 mm from the clamping and measuring the available force (or blocking force F_b) at this point when the structure is activated. This last test is performed on a universal test machine MTS 20 (from MTS), and by using Testworks4 software (load cell capacity: 10 N, accuracy: 10^{-3} N). The temperatures on the CBCM area (T_{sup}) and on the lower side of the beam, below the patch, (T_{inf}) are measured by thermocouples. T_{sup} and T_{inf} are the average of four values measured of each side. A direct current is used to supply electricity to the active area. By using the data at 130 mm from the clamping, the cantilever bending test is also used to obtain the rigidity K of the two structures CBCM-A and CBCM-B (Table 1).

2.2. Active Structure Characterizations. In Figure 3, response curves (free displacement and blocking force versus time) are presented for CBCM-B. Mean curves were calculated from ten tests and for several current intensities (0.8, 1.2, and 1.6 A). At the very first moments of the test, some negative values of free deflection (or blocking force) can be observed. They are due to the existence of an uncontrolled gradient effect, the thermal expansion of the aramid reinforcements is greater than the one of the UD glass layers: the beam bends to negative values. When the temperature tends to be uniform, the thermal expansion of the glass reinforcements is equal and then greater than the one of the aramid layers: the whole structure bends in the opposite direction. This effect is classical for thick CBCM structure and can be solved by an appropriate position of the active layer in the thickness of

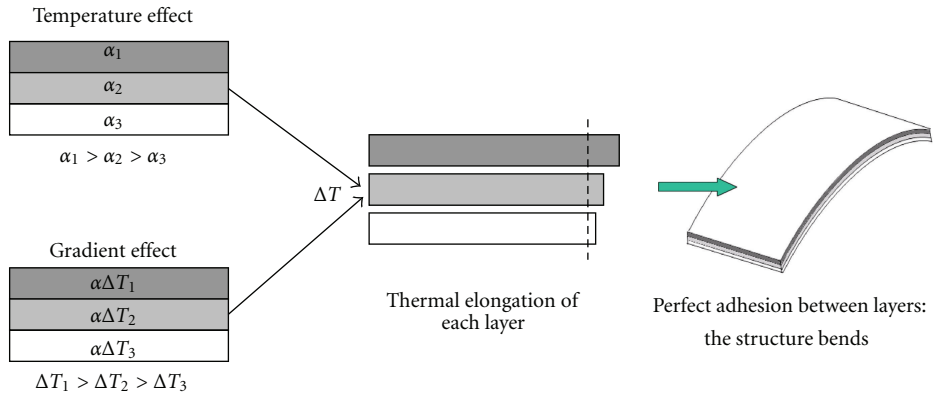

Figure 1: CBCM principle, α_i thermal expansion coefficient.

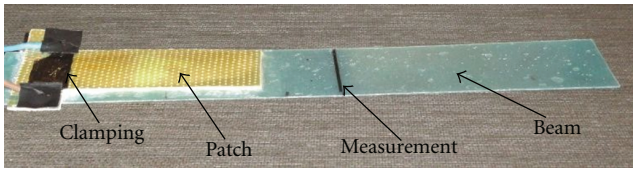

Figure 2: Thermaly active patch.

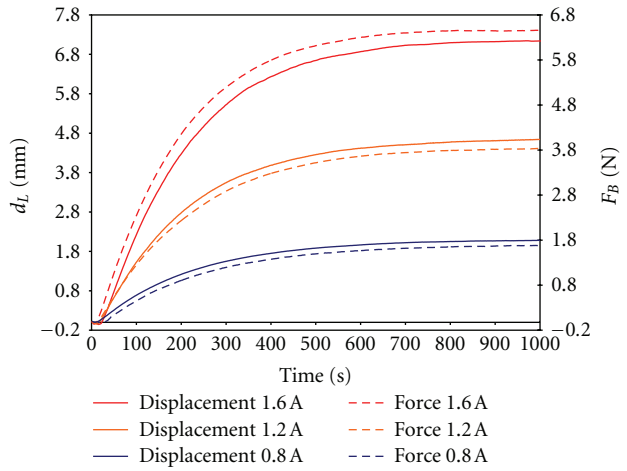

Figure 3: Characteristics curves versus time, free displacements, and blocking forces.

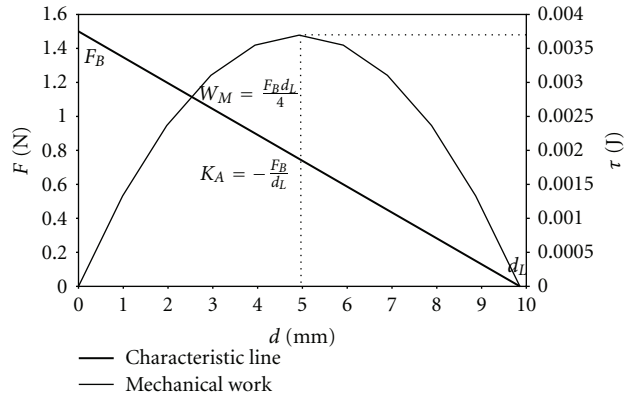

Figure 4: Characteristic straight line and useful mechanical work.

the CBCM laminate [20]. In the present case, because of the use of a thin external active patch there is no other possibility. However, the gradient effect has no importance on the global response of the structure.

After stabilization, the maximum value of the free displacement d_L (or the blocking force F_b) is obtained by the average of the data, recorded during the last 60 s. d_L and F_b are linked by the active rigidity K_A (Figure 4). The characteristic straight line of the active beam highlights the properties of activation given by the free displacement and the blocking force. After activation, and compared to the initial configuration, the free displacement is the maximum value of displacement that the beam can reach without being loaded. The blocking force is the maximum value of force that the beam can support when maintaining its initial configuration. For these two quantities the associated useful work W is equal to zero.

For each value of the displacement d, the useful work W can be calculated (1). This work shows a maximum value W_M (Figure 4), corresponding to a maximum of actuation capability. For each structure, this maximum is associated to a couple of values, displacement $d_M = d_L/2$ and force $F_M = F_B/2$, so the active structure can move a load F_M along a distance d_M

$$F = F_B\left(1 - \frac{d}{d_L}\right), \qquad W = Fd = F_B d\left(1 - \frac{d}{d_L}\right). \tag{1}$$

Like a spring, the total energy of actuation is defined (2). To compare actuation property, this value can be divided by the mass of the structure: E_A^m

$$E_A = \frac{1}{2}K_A d_L^2 = \frac{F_B d_L}{2}. \tag{2}$$

If we do not consider the very first moments of the response, the composite structure reacts like a first-order system. In such problem, it is typical to define the response time τ (time necessary to reach 63% of the maximal response) and the

Table 2: Properties of activation.

Beam	Current (A)	d_L (mm)	sd_P (mm)	sd_F (mm)	F_B (N)	sd_P (10^{-3}N)	sd_F (10^{-3}N)	K_A (10^{-3} N/m)
CBCM-A	0.8	1.45	0.01	0.010	0.540	4	7	0.37
	1.2	3.07	0.08	—	1.107	4	7	0.36
	1.6	4.18	0.04	—	1.820	5	8	0.43
CBCM-B	0.8	1.96	0.03	—	1.790	20	8	0.91
	1.2	4.64	0.05	0.016	3.840	50	20	0.82
	1.6	7.15	0.07	0.016	6.460	70	10	0.90

Table 3: Properties of activation.

Beam	Current (A)	τ_M (10^{-3} J)	E_A (10^{-2} J)	E_A^m (J/kg)	t_s (s)	P_A (10^{-5}W)	P_{el} (W)	η (10^{-6})
CBCM-A	0.2	0.39	1.12	0.58	618	1.81	3.15	5.74
	0.3	1.69	4.85	2.55	543	8.93	7.09	12.59
	0.4	3.80	10.86	5.71	480	22.62	12.62	17.92
CBCM-B	0.2	1.75	3.65	0.76	732	4.98	2.79	17.84
	0.3	8.90	18.56	3.86	645	28.77	6.29	45.73
	0.4	23.00	48.11	10.00	645	74.58	11.18	66.70

characteristic time or stabilized time $t_s = 3\tau$ (time necessary to reach 95% of the maximal response).

So it is possible to define a power of activation P_A and the efficiency η of the active structure (3), where P_{el} is the given electrical power

$$P_A = \frac{E_A}{t_s}, \qquad \eta = \frac{P_A}{P_{el}}. \tag{3}$$

3. Experimental Results

3.1. Stabilized Actuation Properties. For a same level of current intensity (Table 2) and compared to CBCM-A (plain weave), d_L and F_B are higher for CBCM-B (UD). For d_L (resp. F_B), two standard deviations are defined. sd_P is a standard deviation in position, obtained from the maximum value of d_L (or F_B) calculated for each of the ten tests. For the same level of activation, it characterizes the ability of the structure to go to the same position or effort. sd_F is a standard deviation in fixity, obtained from the mean curve and from the average of the data, recorded during the 60 s. It characterizes the ability to the structure to maintain a given position or effort. The values of sd_p and sd_F show the great accuracy of the CBCM structure (nonindicated values are lower than the accuracy of the displacement sensor).

For the two structures, the stiffness of the beam in an active state K_A is smaller than its stiffness K in a nonactive state, 23% smaller for CBCM-A and 19% smaller for CBCM-B, despite a greater stiffness for the CBCM-B (ratio of 2.1). For this last structure, the CBCM effect is more efficient. The use of K_A is well adapted to the characterization of thermaly active composites, because it is a structural characteristic which encompasses the influence of several phenomena: for the matrix, the loss of stiffness versus temperature; for the structure, the geometrical rigidity induced by its curvature during the activation.

Table 4: Comparison to actuators (1.6 A, $E_A = 5.71$ J/kg CBCM-A, $E_A = 10$ J/kg CBCM-B).

Actuator	Mass (g)	d_L (mm)	F_B (N)	E_A (J/kg)
Electromagnet	50	5	2–35	0.2–3.5
Electric motor	200	50	12	3

In Table 3 the characteristic mechanical properties are presented. In term of useful work τ_M and activation energy E_A, the performances are again greater for the CBCM-B. This result highlights the principle of CBCM: contrary to other classical actuators, the CBCMs do not fight against the structural rigidity, the thermal activation turns the whole structure into an actuator. If an appropriate choice for the organization of reinforcements is made, the stiffness of the structure is not a limit to the performances. The CBCM-B has the greater rigidity, but the unidirectional fibers are along the transverse direction of the beam. This choice induces two advantages on the CBCM effect: firstly it gives more importance to the matrix dilatation along the longitudinal direction and secondly it limits the transversal curvature after activation.

In order to simplify mechanisms, CBCM structure can be a substitute to classical actuators, because for the same level of d_L and F_B, the value of E_A (in J/kg) is on the same scale (Table 4). However, due to the thermal activation, one of the main problems that remain is the response time and, as a consequence, the efficiency of the system η (Table 3).

3.2. Active Structure Responses. The response curves of the free displacement and the blocking force are linked to the

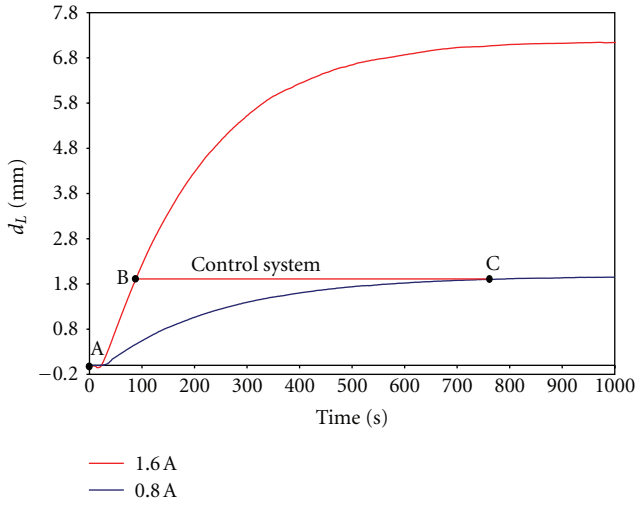

Figure 5: CBCM-B response time.

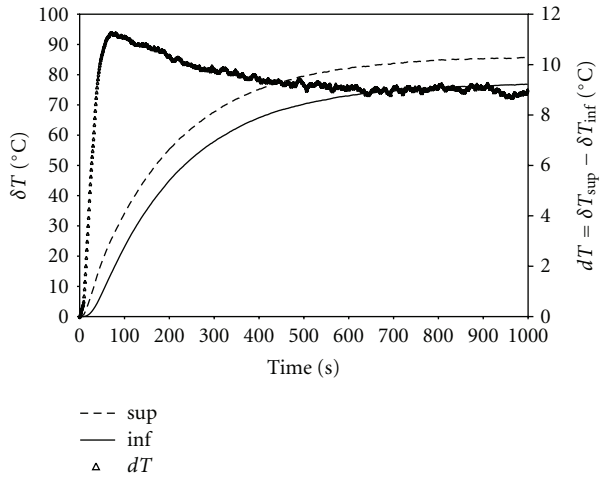

Figure 6: Thermal response of active structure.

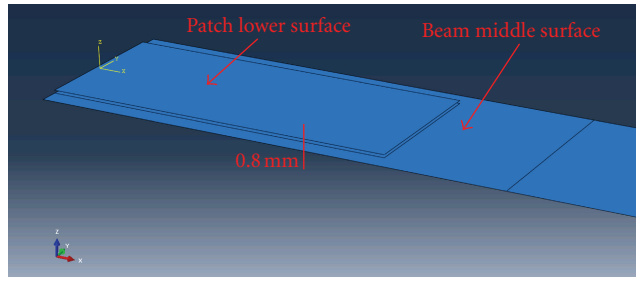

Figure 7: CBCM modelling.

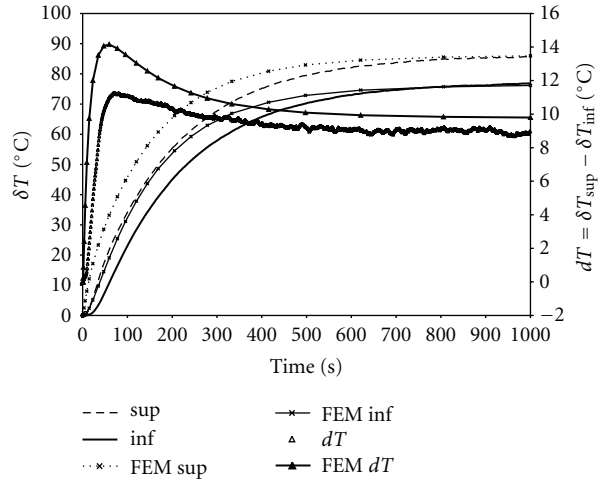

Figure 8: Temperature elevation δT, experimental and FEM.

level of current intensity in the active layer (Figure 1). For the final value of d_L and F_B but also for the slope at the origin, the higher the intensity is, the higher the slope at the origin is.

A solution to reduce the response time is to have, at the beginning, a high level of intensity, and when the prescribed value of d_L (Figure 5) is reached (point C), to use a control system to maintain the value of d_L. Without any control system the path is given by the curve (A, C). With a control system, the path becomes (A, B, C), and the new stabilized time t_s is given by the point B.

For CBCM-B, the value of t_s is indicated in Table 5. For the free displacement and a current intensity equal to 0.8 A ($d_L^{0.8} = 1.96$ mm, $t_s = 732$ s, $\eta^{0.8} = 17.8410^{-6}$), the new values of t_s are $t_s = 130$ s for 1.2 A (42.24% of $d_L^{1.2}$) and $t_s = 91$ s for 1.6 A (27.41% of $d_L^{1.6}$). The corresponding values for η are $\eta^{1.2} = 210^{-5}$ (ratio of 1.12) and $\eta^{1.6} = 310^{-5}$ (ratio of 1.7). It is a good solution to increase the efficiency of the system; however, two problems have to be solved.

The first is to design an adapted control system; it needs an identification of the transfer function [21, 22]. The second is linked to the thermal problem, which is an unsteady problem with a temperature distribution through the composite thickness.

At the beginning of the activation (Figure 6), a difference of response time can be observed between the temperature of the patch on its upper surface $\delta T_{sup} = T_{sup} - T_{room}$ (room temperature $T_{room} = 20°C$) and the temperature on the lower surface of the beam beside the patch ($\delta T_{inf} = T_{inf} - T_{room}$). This phenomenon is induced by a thermal inertial through the thickness of the composite. The curve $dT = \delta T_{sup} - \delta T_{inf}$ can be divided into two parts: an unsteady part with a maximum value for a time of approximately 80 s and for a time greater than 500 s, a stationary part corresponding to the gradient stabilization. This thermal gradient induces a temperature distribution through the thickness of the composite, [distribution linked to the level of current intensity used to activate the composite structure.] So if we want to increase the response time of the structure, this gradient is a limit for the use of high level of intensity because it can induce problems of local over heating and consequently, damage problems.

Table 5: Response system amelioration.

Current		1.2 A				1.6 A			
	Parameter	t_s	% d_L	t_s	% F_B	t_s	% d_L	t_s	% F_B
	(units)	(s)	(%)	(s)	(%)	(s)	(%)	(s)	(%)
0.8 A	d_L (mm)	130	42.24	—	—	91	27.41	—	—
	F_B (N)	—	—	149	46.61	—	—	77	
1.2 A	d_L (mm)	—	—	—	—	225	64.89	—	—
	F_B (N)	—	—	—	—	—	—	179	59.44

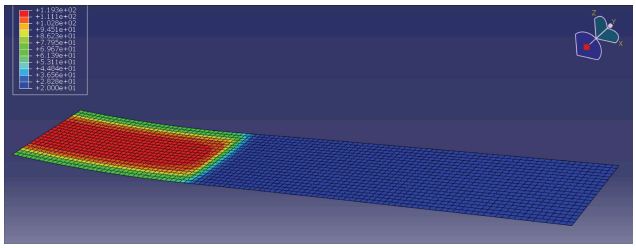

Figure 9: Temperature distribution at the interface.

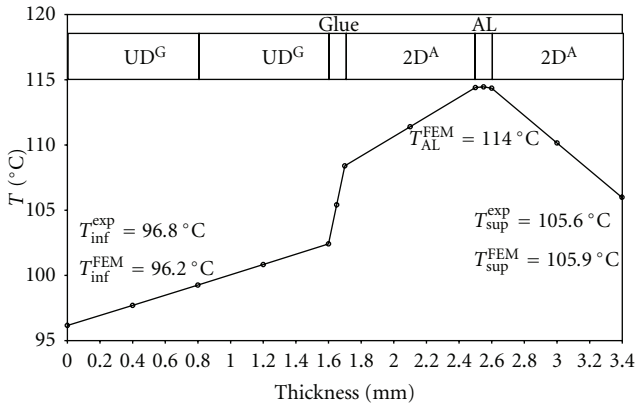

Figure 10: Temperature distribution through the thickness.

4. FEM Procedure

4.1. Model Description

4.1.1. Geometrical Description. One of the main interests of the use of a thermaly active patch is the capability to turn any composite structure into an active structure thanks to a local effect. For this reason, and in order to take into account the real design of the composite structure, we propose an adapted procedure of modelling. Only the CBCM-B will be treated here.

An unsteady thermomechanical calculation using finite elements (Abaqus) has been performed. The beam and patch thickness are measured after manufacturing. In Table 6, the thickness e and the reinforcement volume ratio v_f of the constitutive layers are indicated.

The composite is modeled by two surfaces, the middle surface for the beam and the lower surface for the patch (Figure 7). The distance between the two surfaces is equal to 0.8 mm (thickness of one unidirectional layer of the beam). An 8-node thermally coupled quadrilateral general thick shell element is used S8RT. Based on a Koiter-Sander shell theory, the interpolation is biquadratic for the displacement and bilinear for the temperature. The interface modelling is made by tie conditions between the two surfaces (in order to link the shell degrees of freedom at the interface beam/patch) and a layer of glue, 0.1 mm thickness for the shell corresponding to the patch surface. The temperature through the structure thickness is computed in 13 integration points (3 integration points by layer).

Table 6: CBCM-B thickness properties.

	UD^G	$2D^A$	AL	Glue
e (mm)	0.8	0.8	0.1	0.1
v_f	0.3	0.2	0.4	—

4.1.2. Material and Layer Properties and Boundary Conditions. The anisotropic thermomechanical behaviour of each layer is obtained by a homogenized step (Table 7). For each surface, a locally anisotropic datum coordinate system is used, which follows the structure deformation. Thanks to the homogenized step, the loss in stiffness versus the temperature for the matrix is taken into account. For the epoxy and methacrylate resins, a linear stiffness variation of 20% is considered for a range of temperature from 20°C to 120°C.

The Joule effect in the active layer is taken into account via an internal heating source ϕ (subroutine HETVAL). We have $\phi = Pe/(S_{ac} \cdot e_{ac})$, where S_{ac} and e_{ac} are, respectively the area and the thickness of the patch and P_e is the electrical power supplied. For the active area, the assumption of a uniform heating is used and the power supplied in the active layer can be easily calculated (4), where R is the total resistance of the active layer, n is the number of active yarns, and i_n is the current intensity in each yarn n

$$P_e = R\left(\sum_{j=1}^{n} i_n\right)^2. \quad (4)$$

For the thermal problem, two heat exchanges are considered, convection and radiation. For convection coefficient, the structure is divided into 4 surfaces: the upper surface of the patch, the upper surface of the beam, the lower surface of the beam which is divided in two surfaces, and the surface below the patch and the rest. For each surface the convection

Table 7: Layer thermomechanical behavior.

Units	ρ (Kg·m^{-3})	c (j·kg^{-1} K^{-1})	E_L (MPA)	E_T (MPA)	ν_{TT}	ν_{LT}	G_{TT} (MPA)	G_{LT} (MPA)	α_L (10^{-5} K^{-1})	α_T (10^{-5} K^{-1})	λ_L (W·m^{-1} K^{-1})	λ_T W.m^{-1} K^{-1}
UDG	1610	1001	25726	7291	0.3	0.3	2604	2604	0.97	4.7	0.3	0.5
2DA	1250	1170	16209	16209	0.1	0.1	1549	1549	1.2	1.2	0.16	0.16
AL	1440	990	154432	5194	0.3	0.3	2138	2138	-6.210^{-3}	5.3	72	0.5
Glue	1210	1100	821	821	0.4	0.4	Isotropic		10	10	Fitting	

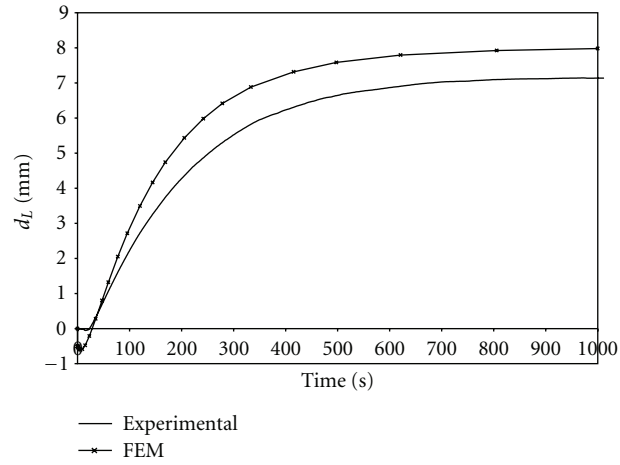

Figure 11: Displacement response, experimental and FEM.

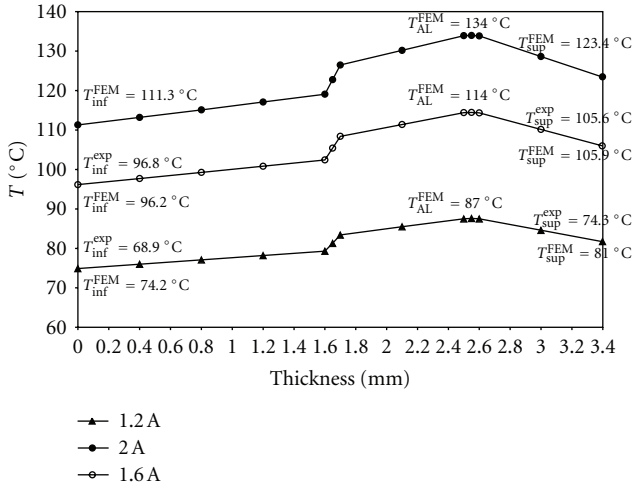

Figure 12: Temperature distribution versus current intensity.

coefficient is calculated thanks to its analytical expression. Then the numerical results are fitting to experimental ones, to adjust the value of the convection coefficients for the upper surface of the patch (T_{sup}), the lower surface of the beam below the patch (T_{inf}). and the conductivity of the glue layer (isotopic behaviour). For the mechanical problem, the gravity is considered and the structure is clamped at one end.

4.2. Comparison between FEM and Experimental Results. In Figure 8, the rise in temperature from the ambient temperature (20°C) is presented versus time. The numerical results are compared to the experimental ones. Because of the fitting procedure, the stationary temperatures are nearly the same. The fitting values for the convection coefficients are, respectively, $h = 11.5\,\mathrm{Wm^{-2}K^{-1}}$ and $h = 9\,\mathrm{Wm^{-2}K^{-1}}$ for the upper surface of the patch and the beam, $h = 4\,\mathrm{Wm^{-2}K^{-1}}$ for the lower surface of the beam and $h = 7.5\,\mathrm{Wm^{-2}K^{-1}}$ for the lower surface of the beam below the patch. For the glue layer the thermal conductivity is $\lambda = 2\ 10^{-2}\,\mathrm{W{\cdot}m^{-1}K^{-1}}$. During the unsteady step, the response time is higher for numerical temperatures. So the thermal inertial linked to the material thermal diffusivity is not taken into account enough by the model. In terms of stabilization and location of maximum value, the numerical and experimental curves of dT are close. For the maximum values, the difference is equal to 3°C.

The temperature distribution at the beam/patch interface (Figure 9) shows that the increase in the temperature is located at the neighborhood of the interface. The principle of thermal local activation is highlighted, and this result is confirmed experimentally. The variation in the temperature through the thickness (Figure 10) shows, on the one hand, an overheating of the active layer: 10°C more than on the upper surface of the patch, and on the other hand, a temperature gap at the interface between the patch and the beam, due to the fitting of the glue conductivity.

For the free displacement response (Figure 11), the model reacts like the experimental system. At the very first moments, we have negative values due to thermal gradient effect, and the value of time stabilization is close to the experimental one. However, we have a difference between the slopes of the two curves during the unsteady response, as between the values for the displacement at stabilization: there is a gap of 11.8% ($d_L^{exp} = 7.14\,\mathrm{mm}$, $d_L^{FEM} = 7.98\,\mathrm{mm}$). This difference is greater for the stabilized value of the blocking force: $F_B^{exp} = 6.47\,\mathrm{N}$, $F_B^{FEM} = 15.4\,\mathrm{N}$.

By the use of two shell structures linked together, this model allows the calculation of a composite structure, being activated thanks to a thermal patch. This model is efficient concerning the temperature evolution versus time and gives useful information on the temperature distribution in the thickness of the composite. For the mechanical value d_L and F_B, the model results are not so good. Concerning the numerical results, the homogenized behaviour is very sensitive, especially the specific heats and the conduction coefficients for the thermal problem and the expansion coefficients for the mechanical problem. The Hashin-Stickman homogenization step may be a cause, so the use of another homogenization scheme is in progress. The modelling choice for the bonding interface may be involved too, but the use of an interface law makes the model more complex to use, particularly for the coefficient identification.

The integrity of the structure and the mechanical performances in terms of response time is linked to the control of the thermal gradient through the thickness. This model can be used for the design of the active patch in order to well adapt its constitution. It can also be used to reduce the response time of the composite, to obtain the thermal distribution through the composite thickness and the limit of the useful current intensity. This is why, for the CBCM-B, we compare at stabilisation (Figure 12) the distribution of temperature through the thickness of the structure for 3 levels of intensity (1.2 A, 1.6 A, and 2 A) 1.6 A is the reference state when we have fitted the data ($\phi = 29\ 10^6\,\mathrm{W{\cdot}m^{-3}}$). For $i = 1.2\,\mathrm{A}$ ($\phi = 21\,\mathrm{W{\cdot}m^{-3}}$) we have a difference between numerical and experimental results, note that the fitting values for heat exchange coefficients are the same as previously mentioned (fitted for $i = 1.6\,\mathrm{A}$). The thermal gradient between the active layer and the upper and lower surfaces is function of the level intensity. So, in order to

decrease the response time of the structure, this modelling tool, coupling to additional experimental tests, can be useful to determine an approximate value for the maximum of intensity that can be used without any damage for the matrix.

5. Conclusion

Only by the use of a thermaly active patch, the results of this study have shown that it is possible to turn any classical composite structure into a morphing structure. For the bonding and to make this technology easy to implement, a methacrylate resin without curing step was used. The mechanical performances of the two CBCM structures are of the same level as that of the performances of classical actuator, motor or jack. Concerning the safety of the composite structure, the use of this technology is well adapted, because it allows concentrating the possible damages around the bonding interface while the rest of the composite structure is safe. The modelling tools we proposed are well adapted for the design of an active structure from a conventional structure. However, some steps of this modelling need some improvement particularly the step of homogenization. Due to the great number of external parameters, the addition of an inverse identification tool seems to be necessary.

References

[1] M. R. Schultz, M. W. Hyer, R. B. Williams, W. K. Wilkie, and D. J. Inman, "Snap-through of unsymmetric laminates using piezocomposite actuators," *Composites Science and Technology*, vol. 66, no. 14, pp. 2442–2448, 2006.

[2] P. Giddings, C. R. Bowen, R. Butler, and H. A. Kim, "Characterisation of actuation properties of piezoelectric bistable carbon-fibre laminates," *Composites Part A*, vol. 39, no. 4, pp. 697–703, 2008.

[3] M. Gude, W. Hufenbach, and C. Kirvel, "Piezoelectrically driven morphing structures based on bistable unsymmetric laminates," *Composite Structures*, vol. 93, no. 2, pp. 377–382, 2011.

[4] W. Hufenbach, M. Gude, and A. Czulak, "Actor-initiated snap-through of unsymmetric composites with multiple deformation states," *Journal of Materials Processing Technology*, vol. 175, no. 1–3, pp. 225–230, 2006.

[5] W. Hufenbach, M. Gude, and L. Kroll, "Design of multistable composites for application in adaptive structures," *Composites Science and Technology*, vol. 62, no. 16, pp. 2201–2207, 2002.

[6] M. L. Dano and M. W. Hyer, "SMA-induced snap-through of unsymmetric fiber-reinforced composite laminates," *International Journal of Solids and Structures*, vol. 40, no. 22, pp. 5949–5972, 2003.

[7] P. F. Giddings, C. R. Bowen, A. I. T. Salo, H. A. Kim, and A. Ive, "Bistable composite laminates: effects of laminate composition on cured shape and response to thermal load," *Composite Structures*, vol. 92, no. 9, pp. 2220–2225, 2010.

[8] F. Mattioni, P. M. Weaver, K. D. Potter, and M. I. Friswell, "Analysis of thermally induced multistable composites," *International Journal of Solids and Structures*, vol. 45, no. 2, pp. 657–675, 2008.

[9] S. Daynes and P. Weaver, "Analysis of unsymmetric CFRP-metal hybrid laminates for use in adaptive structures," *Composites Part A*, vol. 41, no. 11, pp. 1712–1718, 2010.

[10] Y. J. Zheng, L. S. Cui, and J. Schrooten, "Basic design guidelines for SMA/epoxy smart composites," *Materials Science and Engineering A*, vol. 390, no. 1-2, pp. 139–143, 2005.

[11] G. Zhou and P. Lloyd, "Design, manufacture and evaluation of bending behaviour of composite beams embedded with SMA wires," *Composites Science and Technology*, vol. 69, no. 13, pp. 2034–2041, 2009.

[12] P. Binette, M. L. Dano, and G. Gendron, "Active shape control of composite structures under thermal loading," *Smart Materials and Structures*, vol. 18, no. 2, Article ID 025007, 2009.

[13] M. L. Dano, M. Gakwaya, and B. Jullière, "Compensation of thermally induced distortion in composite structures using macro-fiber composites," *Journal of Intelligent Material Systems and Structures*, vol. 19, no. 2, pp. 225–233, 2008.

[14] F. Laurent, "Continuously deformable and controllable composite material," WO 2005084936, 2005.

[15] H. Drobez, G. L'Hostis, K. Gautier, F. Laurent, and B. Durand, "A new active composite," *Smart Materials and Structures*, vol. 18, Article ID 025020, 2009.

[16] K. B. Gautier, G. L'Hostis, F. Laurent, and B. Durand, "Mechanical performances of a thermal activated composite," *Composites Science and Technology*, vol. 69, no. 15-16, pp. 2633–2639, 2009.

[17] G. Trakakis and C. Galiotis, "Development and testing of a self-deformed composite material," *Composite Structures*, vol. 92, no. 2, pp. 306–311, 2010.

[18] H. Asanuma, O. Haga, J. I. Ohira, G. Hakoda, and K. Kimura, "Proposal of an active composite with embedded sensor," *Science and Technology of Advanced Materials*, vol. 3, no. 2, pp. 209–216, 2002.

[19] H. P. Monner, "Smart material for active noise and vibration reduction," in *Proceedings of the Noise and Vibration Emerging Methods*, pp. 18–21, Saint Raphael, France, April 2005.

[20] H. Drobez, G. L'hostis, K. Buet Gautier, F. Laurent, and B. Durand, "Thermomechanical modelization of a new active material," *Journal of Intelligent Material Systems and Structures*, vol. 20, no. 13, pp. 1541–1552, 2009.

[21] A. Collaine, J. M. Freyburger, G. l'Hostis, F. Laurent, and B. Durand, "The controlled behaviour of composite material model for control," *Experimental Techniques*, vol. 33, no. 5, pp. 44–49, 2009.

[22] A. Collaine, J. M. Freyburger, and B. Durand, "CBCM thermal and electrical properties identification and proposition for the control," in *Proceedings of the 11th AUTEX World Textile Conference*, June 2011, session poster.